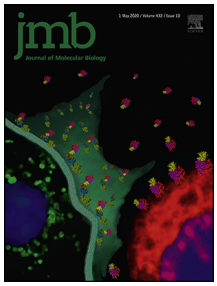

A Generalizable Optogenetic Strategy to Regulate Receptor Tyrosine Kinases during Vertebrate Embryonic Development

Vishnu V. Krishnamurthy[1,†], Jia Fu[2,†], Teak-Jung Oh[1], John Khamo[1,‡], Jing Yang[2] and Kai Zhang[1,]

*1 - **Department of Biochemistry,** University of Illinois at Urbana-Champaign, Urbana, IL 61801, USA*
*2 - **Department of Comparative Biosciences,** University of Illinois at Urbana–Champaign, Urbana, IL 61802, USA*

***Correspondence to Jing Yang and Kai Zhang:** J. Yang is to be contacted at: 2001 S Lincoln Ave, VMBSB3411, Urbana, IL 61802, USA; K. Zhang is to be contacted at: 600 South Mathews Avenue, 314 B Roger Adams Laboratory, Urbana, IL 61801, USA. yangj@illinois.edu, kaizkaiz@illinois.edu*
https://doi.org/10.1016/j.jmb.2020.03.032
Edited by Dr M Yaniv

Abstract

Ligand-independent activation of receptor tyrosine kinases (RTKs) allows for dissecting out the receptor-specific signaling outcomes from the pleiotropic effects of the ligands. In this regard, RTK intracellular domains (ICD) are of interest due to their ability to recapitulate signaling activity in a ligand-independent manner when fused to chemical or optical dimerizing domains. A common strategy for synthetic activation of RTKs involves membrane tethering of dimerizer–RTK ICD fusions. Depending on the intrinsic signaling capacity, however, this approach could entail undesirable baseline signaling activity in the absence of stimulus, thereby diminishing the system's sensitivity. Here, we observed toxicity in early *Xenopus laevis* embryos when using such a conventional optogenetic design for the fibroblast growth factor receptor (FGFR). To surpass this challenge, we developed a cytoplasm-to-membrane translocation approach, where FGFR ICD is recruited from the cytoplasm to the plasma membrane by light, followed by its subsequent activation via homo-association. This strategy results in the optical activation of FGFR with low background activity and high sensitivity, which allows for the light-mediated formation of ectopic tail-like structures in developing *X. laevis* embryos. We further generalized this strategy by developing optogenetic platforms to control three neurotrophic tropomyosin receptor kinases, TrkA, TrkB, and TrkC. We envision that these ligand-independent optogenetic RTKs will provide useful toolsets for the delineation of signaling sub-circuits in developing vertebrate embryos.

Introduction

Among the various proteins that inhabit the plasma membrane, the receptor tyrosine kinase (RTK) family forms a subset of integral membrane proteins that transmit signals across the membrane [1]. They transduce signals for the regulation of major cellular processes, including survival, proliferation, differentiation, motility, metabolism, and even death. In multicellular organisms, RTK signaling plays key roles in early and late development as well as in organogenesis [2,3]. A prototypical structure shared by RTKs includes an extracellular domain, a single membrane-spanning helix, and an intracellular domain (ICD) possessing the tyrosine kinase activity. Whether RTKs exist as monomers or preformed dimers is contested, with evidence supporting proponents of both these models [4] depending on the identity of the RTK. Ligand-binding forces either the dimerization of monomers or a rearrangement of inactive dimers into a conformation that brings the ICDs of two units into proximity. The active state of the RTKs is a dimer where the intracellular domains are aligned properly. This alignment activates the tyrosine kinase domain and entails the trans-autophosphorylation of multiple tyrosine sites in the ICD [1]. In turn, these phosphorylated tyrosines serve as docking sites for various adapter proteins, which activate the downstream signaling effectors for distinct signaling pathways. Interestingly, many of

these proteins are shared across RTKs. Not surprisingly, the subsets of pathways activated by different RTKs also overlap. For example, the fibroblast growth factor receptor (FGFR) and the neuronal Trk family receptors (Trks) activate the mitogen-activated protein kinase, AKT, and phospholipase C γ (PLCγ) pathways in response to their respective ligands fibroblast growth factor (FGF) and nerve growth factor (NGF) [5].

Despite activating receptors with similar signaling characteristics, different ligands elicit differences in phenotypic outcomes when applied to cells. Whereas both FGF and NGF induce differentiation of PC12 neuroblasts with continuous stimulation [6,7], discontinuous stimulation revealed two phases in differentiation with a strict dependence on NGF, where FGF cannot replace NGF in either phase [8]. Whether this distinction arises from an intrinsic difference in the signaling capacity of receptors or the pleiotropic effects of the ligands is unclear. For example, NGF can interact with two receptors, namely TrkA and p75NTR, with high and low affinities, respectively [9,10]. Activation of either receptor elevates the activity of ERK, a primary effector of PC12 cell differentiation. Hence, one possible explanation for the differential signaling responses to NGF and FGF discontinuous stimulation in PC12 cells may be the pleiotropic effects of NGF. Another possibility lies in the differences in the innate signaling capacities of their receptors, which remains to be explored. These explanations are not mutually exclusive and may have to be taken together to explain the differential phenotypic outcomes of the ligands. The contribution of individual receptors to signaling needs to be ascertained to better understand the links between ligands and the end-point responses.

To distinguish the pleiotropic effects of the ligand from receptor-specific signaling and to assess receptor-specific contributions to signaling, ligand-independent activation of the receptors is desirable. Chemogenetic and optogenetic approaches that activate RTKs have been developed, where the receptors are fused to chemical-responsive or light-responsive modules, respectively [11–18]. We and others have developed optogenetic approaches to activate TrkA and FGFR in a ligand-independent fashion [11–13,15,19]. A common design in these optogenetic systems involves the fusion of intracellular domains (ICDs) of RTKs to an optogenetic component, commonly anchored on the plasma membrane via a myristoylated moiety.

The membrane-anchored, ligand-independent RTK activation system is very informative in uncovering the fine nuances of signaling, which are simply not accessible with ligand application. Depending on the intrinsic signaling capacity of the RTK ICD, however, membrane-associated RTK risks elevating the baseline signaling activity. Indeed, we observed high basal activity for a membrane-targeted optoTrkA in a previous study [13]. We speculate that the undesirable high background activity could result from targeting of the myristoylated/palmitoylated RTK ICD to "lipid-raft" microdomains, where the high local concentration of these receptors and other signaling components favors strong signaling activity even in the absence of a stimulus [20,21]. Achieving the desired signaling output with these synthetic RTKs often requires fine-tuning of construct expression levels or doping with inactive constructs to maintain low baseline levels of activity. These compensatory measures normally applied to cultured mammalian cells are unfeasible in complex multicellular systems such as developing embryos.

We sought to build optogenetic RTKs with low basal activity and high light sensitivity for application in tissues and organisms. Since membrane localization is key to the activation of RTKs, we optimized a translocation system that shuttles RTK ICDs to the plasma membrane with light. We made use of the blue light-inducible pair from *Arabidopsis thaliana* consisting of the cryptochrome 2 (CRY2) photolyase homology region (PHR) and cryptochrome-interacting basic helix–loop–helix N-terminal domain (CIBN) [22]. We designed a plasma membrane-anchored CIBN and the RTK-ICD fused to CRY2, with the expectation that the ICDs will be recruited to the plasma membrane with blue light. Furthermore, we reasoned that the homo-association of the recruited CRY2 at the membrane would contribute to ICD dimerization or multimerization and its activation. To maintain a low baseline activity, we also employed a non-lipid raft targeting farnesyl modification (CaaX) [21] to anchor the CIBN construct to the plasma membrane.

Results

Membrane-associated optoFGFR is functional in mammalian cells but causes premature death in *Xenopus laevis* embryos

We first tested a conventional design of optoFGFR, Lyn-FGFR-AuLOV-EGFP, where a membrane-associated optical dimerizer (AuLOV) [13] was fused to the intracellular domain of FGFR (Figure 1(a)). Because we observed high basal activity in the dark in HEK293T cells, we systematically doped our transfections with a signaling-inactive construct Lyn-AuLOV-EGFP (ICD-empty), which lacked the FGFR ICD. The FGFR:ICD-Empty mass ratio was tuned from 1:11 to 6:6 (Figure 1(b)). Although we observed an increase in the phosphorylation of ERK, AKT, and PLCγ, three canonical downstream signaling proteins, the baseline levels of each phospho-target were not effectively

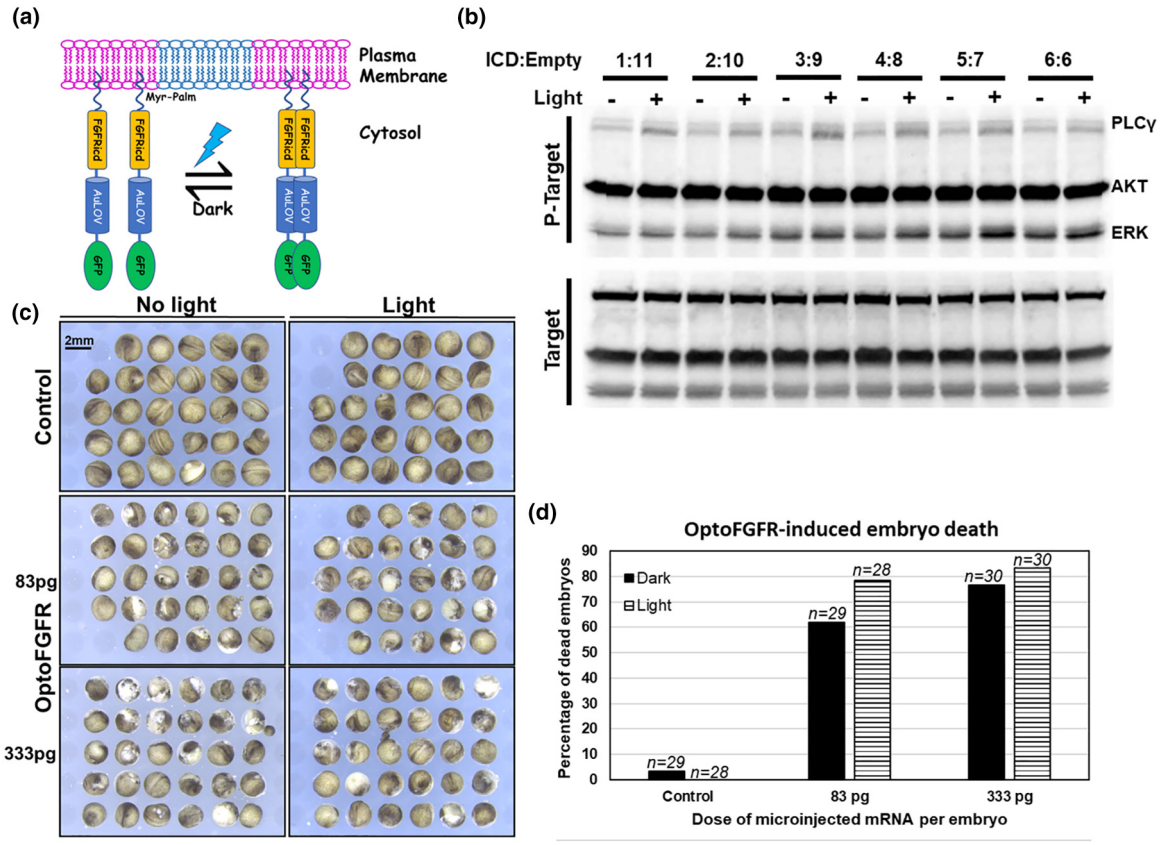

Figure 1. Membrane-associated OptoFGFR system causes early embryonic death during *Xenopus* development. (a) Schematic of the optoFGFR construct and its proposed mechanism of action. Myristoylated and palmitoylated FGFRicd targets preferentially to lipid rafts (magenta). The LOV domain enables reversible dimerization under blue light. (b) Western blots of the construct in (a) 24 h after transfection into HEK293T cells, lysed after a 5-min blue light illumination at 5 mW/cm^2 in the presence of the EGFR inhibitor Erlotinib (10 μM), and probed for the phosphorylation of ERK, AKT, and PLCγ. The blot on the top shows phosphorylated targets, while the bottom blot shows corresponding total targets. The optoFGFR construct was co-transfected with an FGFRICD-lacking version of the construct to attenuate the hyperactivity of the ICD-bearing construct that likely stemmed from its efficient localization to lipid rafts; the ratios on top indicate the ICD to non-ICD plasmid ratio where the total DNA transcfected was set as 1.2 μg across all the conditions tested. (c) Expression of the construct in (a) was constitutively toxic to *X. laevis* embryos even when its mRNA was microinjected at low doses and even when there was no blue light illumination, as seen from the uneven distribution of pigmentation in dead embryos. (d) Quantification of *X. laevis* embryo death after OptoFGFR microinjection.

lowered even at a 1:11 ratio of FGFR: ICD-Empty vector (Figure 1(b)). In particular, the baseline AKT activity was so strong that we could not observe further enhancement upon light stimulation (Figure 1(b)).

We hypothesized that such high activity from membrane-associated optoFGFR could be detrimental for *in vivo* applications. To test this idea, we micro-injected 333 pg *in vitro*-transcribed Lyn-FGFR-AuLOV-EGFP mRNA into *X. laevis* embryos at the four-cell stage and examined the phenotypic effects of light and dark incubations on their development. Since hyperactivation of the ERK pathway in *Xenopus* embryos has been shown to induce ectopic tail-like structures [23,24], we anticipated analogous outgrowths in optoFGFR-microinjected embryos upon maturation. However, embryos injected with Lyn-FGFRICD-AuLOV-EGFP barely survived till the neurula stage, even when incubated in the dark (Figure 1(c), unevenly pigmented embryos in bottom panels). Lowering the dose of mRNA to 83 pg did not significantly improve embryo survivability, suggesting hyper signaling activity that is toxic to embryos (Figure 1(c), middle panels). In contrast, in our previous studies, we could use up to 500 pg of optogenetic Raf1 mRNA without observing detectable embryonic death [24]. These results indicate that, despite blue light-induced enhancements in ERK signaling from the membrane-associated optoFGFR in cultured mammalian cells, its high basal activity renders it impracticable in whole embryos, which may have a lower tolerance threshold for hyperactive FGFR signaling.

Cytoplasm-to-membrane translocation-based optoFGFR activates the canonical FGF signaling in mammalian cells

To address the hyperactivity issue of the membrane-associated optoFGFR, we took inspiration from a recent work [25] to develop a cytoplasm-to-membrane translocation scheme for activating FGFR. The construct, CRY2PHR-mCherry-FGFRICD-P2A-CIBNx2-EGFP-CaaX, uses the viral-derived P2A peptide to generate two stoichiometric polypeptides from a single transcript [26]. This construct will be referred to as "CMT-OptoFGFR" (cytoplasm-to-membrane translocation) hereon (Figure 2(a)). This system is similar to a construct we designed to activate Raf1 in mammalian cells and *Xenopus* embryos [24]. Epifluorescence microscopy confirmed that the CIBNx2-EGFP-CaaX (CGC) and CRY2PHR-mCherry-FGFRICD (CmF) localized to the correct intracellular compartments. Pulsing of blue light caused a rapid translocation of CmF to the plasma membrane (Figure 2(b) and (c)). Because of the suboptimal photostability of mCherry, its fluorescence intensity was reduced after light exposure both on the plasma membrane and in the cytoplasm (Figure 2(c), right panels). However, the relative membrane-to-cytosolic intensity ratio increased after light exposure, indicating membrane translocation of mCherry-fusion proteins. Because activation of FGFR leads to the upregulation of c-Fos transcription, we used a *firefly* luciferase reporter driven by a c-Fos promoter to assess if the translocation of ICD could activate canonical FGFR signaling [27,28]. As expected, CMT-OptoFGFR showed a robust increase in luciferase activity with light (Figure 2(d)). We next asked if CMT-OptoFGFR can induce the differentiation of PC12 neuroblasts like the natural FGF ligand. We observed that CMT-OptoFGFR promoted strong neurite outgrowth with light while being almost completely

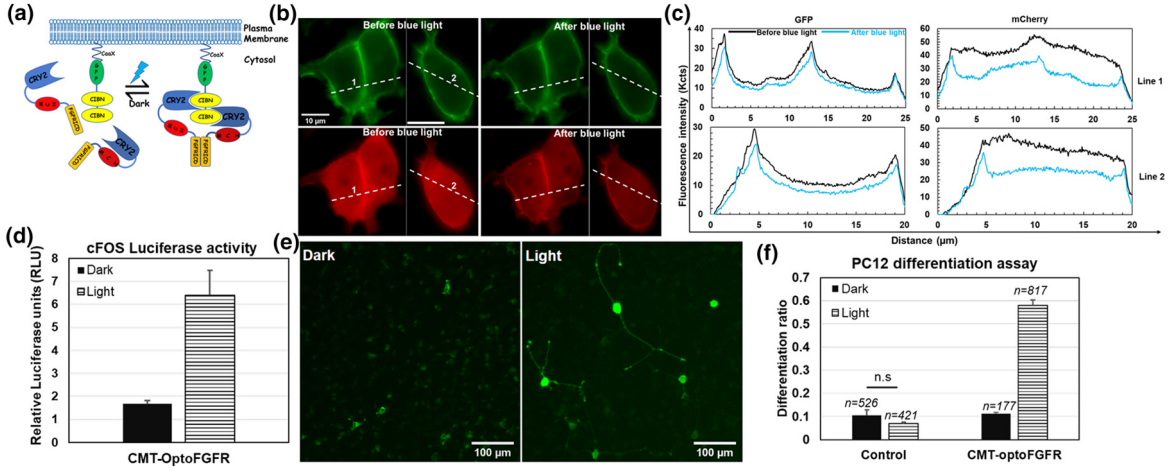

Figure 2. Construction and validation of the CMT-OptoFGFR system. (a) Schematic of the CMT-OptoFGFR construct and its putative mechanism of action. Cytosolic CRY2-mCherry-FGFRICD is reversibly recruited to plasma membrane-anchored CIBN with blue light and subsequently self-associates via the double-CIBN. (b) Epifluorescence microscopic images of CMT-OptoFGFR in transfected HEK293T cells. Cells plated on glass coverslips were transiently transfected and imaged after 24 h. Images from the GFP and mCherry channels were recorded after administration of short (100 ms) blue light (488 nm) pulses using the microscope. (c) Intensity plot profiles of lines 1–2 represented in (b). Pre-blue light profiles (black) and the post-blue light profiles (blue) are indistinguishable for GFP, whereas the mCherry distribution shifts from relatively homogeneous plateaus across the cell to focused peaks of increased intensity at the edges corresponding to the location of the plasma membrane. The decrease in absolute intensity values of the blue line comes from photobleaching (d) cFOS luciferase assay for HEK293T cells grown in 24-well plates and transiently transfected with 100 ng CMT-OptoFGFR along with plasmids encoding for cFOS promoter-controlled luciferase reporter (50 ng), a Renilla luciferase (control reporter), and a filler plasmid (310 ng) to a total of 500 ng per well. Twenty-four hours following transfection, the cells were serum-starved to minimize background signaling activity and concomitantly illuminated for 18 h with 400–500 μW/cm^2 blue light (460 nm), and luciferase activity was measured. Relative luminometer units (RLU) were obtained as the ratio of Firefly to Renilla luminescence counts. Values represent mean ± s.d. of triplicate measurements (n = 3). (e) Representative epifluorescence images of CMT-optoFGFR-transfected cells showing long-neurites under light-incubation. PC12 NS1 cells grown in 24-well plates were transfected with 500 ng of plasmid encoding optoFGFR or CIBN-GFP-CaaX (negative control). Following 24 h, the cells were serum-starved and illuminated for 48 h with 400 μW/cm^2 blue light (460 nm) from a custom-built LED array mounted beneath the culture dish placed inside the incubator, and then imaged. Cells incubated in the dark show little to no neurite outgrowth. (f) Quantification of PC12 cell differentiation with CMT-OptoFGFR. Differentiation ratio was defined as the ratio of transfected cells showing neurite outgrowth over the total pool of transfected cells. The data were quantified manually using the ImageJ software. The data represent two biological replicates. The total number of cells counted is indicated on the bar graph. n.s. = not significant.

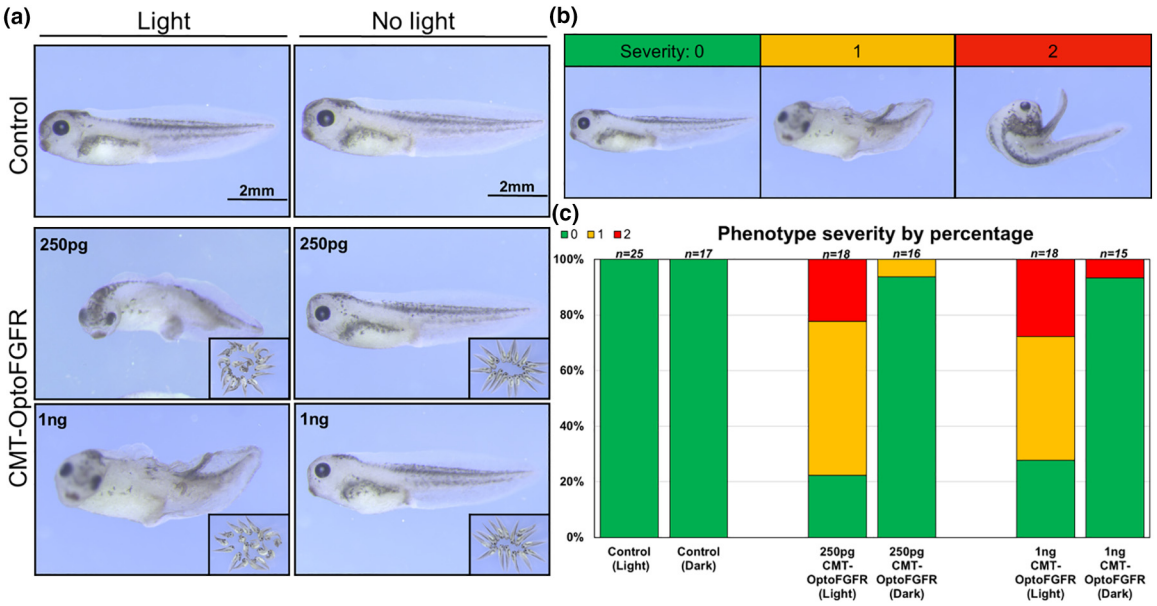

Figure 3. Optogenetic activation of FGFR signaling induces ectopic structures in *X. laevis* embryos. (a) CMT-OptoFGFR activation induces ectopic tail-like structures in *Xenopus* embryos. Fertilized frog eggs were mock-injected or microinjected with the indicated dose of *in vitro*-transcribed OptoFGFR mRNA and continuously illuminated with 5 mW/cm^2 blue light. Images were taken at the tailbud stage. Ectopic tail-like structures are clearly visible in the illuminated embryos. Inset images present more embryos of the indicated condition. (b) Representative images of phenotype severities. (c) Stacked bar graphs quantifying the severity of light-induced phenotype in OptoFGFR-expressing embryos.

inactive in the dark (Figure 2(e) and (f)). These results demonstrate that CMT-optoFGFR is a fully functional blue light-induced signaling switch.

CMT-OptoFGFR shows minimal toxicity and induces ectopic tail-like structures in *X. laevis* embryos

We then examined if CMT-OptoFGFR was functional in developing *X. laevis* embryos. We have previously demonstrated that an optogenetic Raf1 is capable of triggering hyperactive mitogen-activated protein kinase signaling to induce an ectopic tail-like structure in *Xenopus* embryos [24]. Others have shown that these tail-like structures can be induced by oncogenic tyrosine kinase receptors, where the combined effect of hyperactive ERK and AKT pathways augments the size of these structures [23]. When CMT-OptoFGFR transcripts were injected into early *X. laevis* embryos and subjected to blue light illumination, these structures readily formed (Figure 3(a)). Remarkably, even high doses of the construct (1 ng mRNA) did not promote these structures in the dark. We could quantitatively assess signaling activity in embryos based on the morphology of embryos by defining an index of severity, where 0 indicates normal morphology, 1 indicates slight deformation of embryonic morphology, and 2 indicates severe deformation (Figure 3 (b)). We observed that there was only a marginal difference between the severity of phenotypes at different doses of microinjection (Figure 3(c)). These results establish CMT-OptoFGFR as a non-toxic and light-sensitive switch applicable to tissue culture cells and embryos.

Development of a generalizable optoRTK platform for *in vivo* studies

We expected that the design principles in CMT-OptoFGFR could be extended to other RTKs such as the neurotrophin receptors TrkA, TrkB, and TrkC. To confirm this idea, we swapped the FGFRICD in CMT-OptoFGFR with the ICDs of TrkA, TrkB, and TrkC to generate CMT-OptoTrkA, CMT-OptoTrkB, and CMT-OptoTrkC, respectively (Figure 4(a)). These new constructs demonstrated their responsiveness to blue light when transfected into HEK293T cells, as evidenced by the translocation of their TrkICDs to the plasma membrane with light. Representative fluorescence images in GFP and mCherry channels of CMT-OptoTrkC before and after blue light stimulation are shown in Figure 4(b) and Supplementary Figure S1. Short pulses of blue light sufficed to translocate TrkCICD-mCherry to the plasma membrane. We then tested the ability of these CMT-OptoTrks to induce transcription of a cFos promoter-driven luciferase reporter. In HEK293T cells, all three Trks induced luciferase activity strongly with light and showed low background activity in the dark (Figure 4(c)). Moreover, all CMT-OptoTrks induced significant PC12 cell

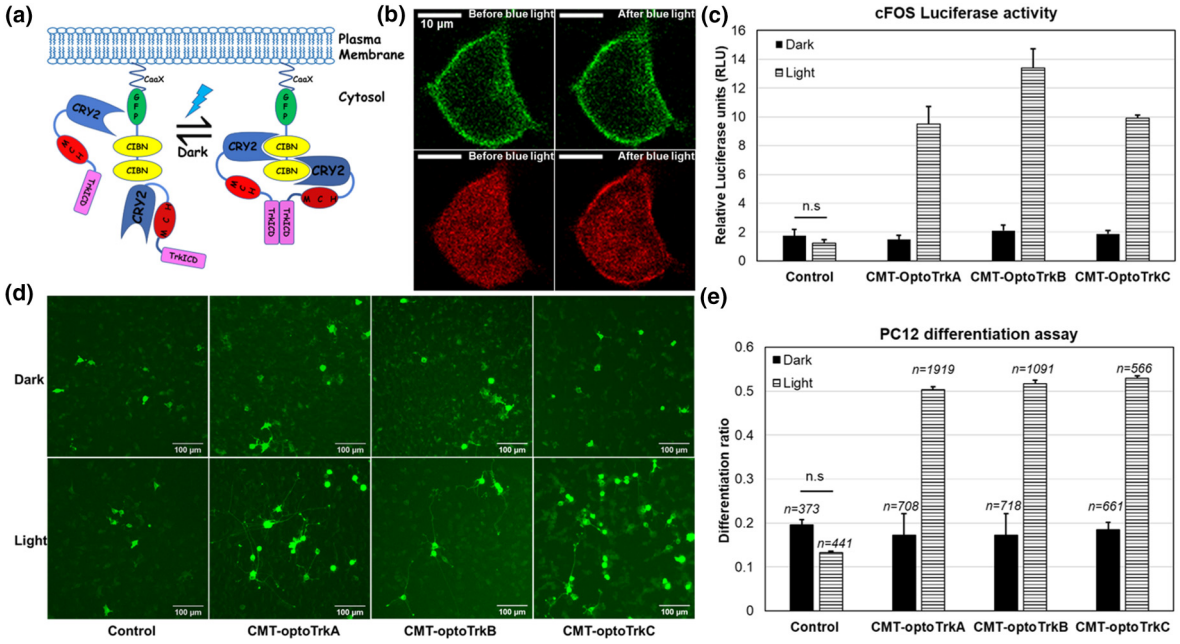

Figure 4. Design and evaluation of the CMT-OptoTrk system. (a) Schematic of the CMT-OptoTrk constructs representing the two-step recruitment and dimerization model of activation explained in Figure 1(a). Trk can be TrkA, TrkB, or TrkC. (b) Confocal microscopic images of live HEK293T cells grown on glass-bottomed petri dishes and transiently transfected with CMT-OptoTrkC. Ten pulses of 1-s blue laser light were delivered via the microscope objective, and the before and after images were recorded. Plasma membrane translocation of cytosolic TrkC after blue light is apparent in the red channel. The green channel visualizes the membrane-anchored CIBN-EGFP module, which marks the plasma membrane and seems unresponsive to blue light. A detailed analysis of the membrane and cytosolic fluorescence profile is presented in Figure S1. (c) cFos luciferase assay for HEK293T cells in 24-well plates transiently co-transfected with plasmids encoding CMT-OptoTrks, cFOS promoter-controlled luciferase, and Renilla luciferase (control), and after illumination and processing as described in Figure 2(d). Values represent mean ± s.d. of three biological replicates. (d) CMT-OptoTrks induce robust PC12 cell differentiation with light. Representative images of CMT-OptoTrk- and CIBN-EGFP-CaaX(control)-transfected PC12 cells following incubation in the light or dark as explained in Figure 2(e). (e) Quantification of PC12 cell differentiation with CMT-OptoTrkA, -OptoTrkB, and -OptoTrkC as in Figure 2(e). The total number of counted cells is indicated on top of the bars.

differentiation with robust neurite extension upon blue light stimulation (Figure 4(d) and (e)), consistent with their neurotrophic role.

We next tested CMT-OptoTrkA and CMT--OptoTrkB in *X. laevis* embryos and observed that both constructs elicited ectopic tail-like structures with light stimulation, consistent with their ability to activate the ERK and AKT signaling pathways (Figure 5(a) and (b)). These results are in consonance with a recent study in *Xenopus* delineating the involvement of TrkA in body axis elongation during embryogenesis and tail elongation during tadpole regeneration [29]. Notably, these ectopic tail-like structures were induced at lower doses (50–200 pg) of CMT-optoTrkA and CMT-optoTrkB when compared with CMT-optoFGFR. Remarkably, CMT-OptoTrkB was able to produce a more severe phenotype when compared to a similar dose of CMT-OptoTrkA (Figure 5(b)). The representative images of different severity and quantitative analysis of the dose-dependent cell phenotype are shown in Figure 5(c) and (d), respectively.

Discussion

In summary, we developed a generalizable optogenetic platform to activate RTKs with the twin goals of achieving low basal activity and high light sensitivity, suitable for application to 2D monolayer cell cultures and 3D embryos. The design is based on the spatial separation of the RTK ICD from the plasma membrane until the application of light, which restores its contact with the membrane and activates it. We reason that cytosolic RTK ICDs are less susceptible to activation due to their alienation from important signaling components such as adaptor proteins and kinases residing on the plasma membrane. Furthermore, the local concentration of these RTK ICDs and their associated signaling

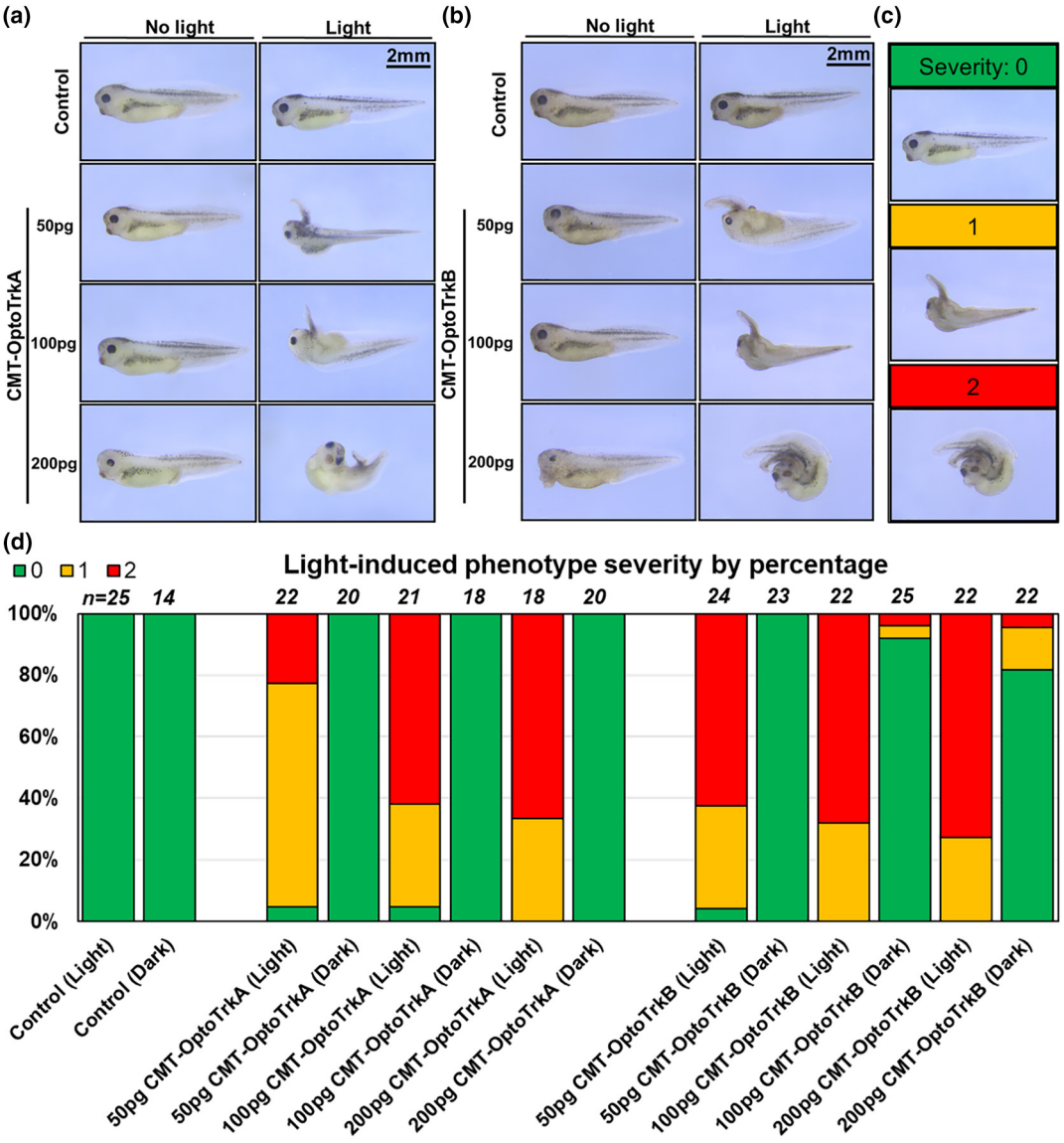

Figure 5. Activation of CMT-OptoTrks induces ectopic structures in *X. laevis* embryos. (a and b) CMT-OptoTrkA or -optoTrkB activation induces ectopic tail-like structures in *Xenopus* embryos, similar to OptoFGFR. (c) A representative legend for the severity of phenotype in injected embryos. (d) Stacked bar graphs quantifying the severity of phenotype in CMT-OptoTrk-expressing embryos.

components in the cytosol is less likely to reach near-activation levels due to the dispersive nature of the cytoplasm. In sharp contrast, the plasma membrane focuses these active signaling molecules into lipid rafts poised for activation. We clearly observed this effect in the case of our lipid-rafted optogenetic TrkA ICD, the activity of which had to be limited by the co-application of lipid-rafted non-ICD optogenetic components to surround the ICD and restrict its unwanted dimerization [13]. Here we used the non-raft farnesyl motif as a cautionary measure to limit dark activity and enhance its switching ability. A recent study tested different strategies for NGF-free TrkA activation using optogenetics [25]. Remarkably, a design almost identical with the optoTrkA used in this study was the most successful in recapitulating the phenotypic effects of the natural TrkA ligand NGF. We propose that our design can be extended to other RTKs, given that their general architecture and their mechanisms of activation and function are similar.

Our experimental results suggest intrinsic but subtle signaling differences between TrkA and TrkB, and between the Trks and FGFR, as witnessed by their different dose-dependent responses in *Xenopus* embryos. These intrinsic differences between receptors must be considered when making comparisons between ligand-induced

phenotypic responses. Disparities in the phenotypic outcomes of NGF- and FGF-induced PC12 differentiation cannot, therefore, be fully attributed to ligand pleiotropic effects alone. One must also take into account the intrinsic capacity of the receptor ICDs, although the former seems to be the more dominant factor. In this regard, an optogenetic approach is advantageous in that it reveals such nuances in signaling by removing the influence of the ligand and offering a level playing field for comparison of RTKs.

An interesting aspect of our construct design is the use of the 2xCIBN module. We have retained this module in our designs due to its efficacy in our previous work with Optogenetic Raf1 where we observed its superiority over the one or three CIBN modules [24]. We were inclined to test if the 2 × CIBN is indeed the optimal module in the context of an optogenetic RTK. In this regard, we modified CMT-OptoTrkA by replacing the 2 × CIBN with 1 × or 3 × CIBN to evaluate their signaling potency. We observed that the 2 × CIBN is indeed the optimal module in this case (Figure S2, Table S1). We propose that this arrangement is either kinetically favorable for CRY2 binding or sterically favorable for maintaining optimal plasma membrane distance for recruited proteins.

We suggest at least two immediate applications for these optogenetic RTKs. First, they can be used to dissect the contribution of a specific RTK to signal transduction without the use of its natural ligand, especially when the ligand is pleiotropic like NGF. Second, mutations can be made to the ICD and its signaling carefully examined without the influence of the overpowering effects of the ligand. Disease-causing mutations deserve mention in this regard. The ability to spatiotemporally confine light and tune its intensity offers a plethora of opportunities for utilizing these tools in studying developmental processes and probing complex multicellular environments. We maintain that a practical limitation with these tools is the light delivery to thicker tissues and whole organisms. Therefore, the onus is on synthetic biologists to develop systems utilizing the deep tissue-permeating red or infra-red light and to invent techniques to deliver light to the interior tissues of organisms. Indeed, a recent system based on bacterial phytochromes allows for near-infrared and far-red light-controlled TrkA and TrkB in mammalian cells and live mice [15].

Materials and Methods

Plasmids

OptoFGFR was constructed by inserting a PCR fragment of the *X. laevis* FGFR1 intracellular domain (NP_001081157.1; residues 394-812) into the KpnI and XbaI sites of pEGFPN1 Lyn-AULOV-EGFP [13]. CMT-OptoFGFR was constructed by restriction digestion of pCS2+ OptoRaf1 [24] with KpnI and Kpn2I, followed by Infusion-cloning with a PCR fragment of *X. laevis* FGFR1 intracellular domain (NP_001081157.1; residues 394-812). CMT-OptoTrkA, CMT-OptoTrkB, and CMT-OptoTrkC were made by inserting the rat TrkA intracellular domain (NCBI NP_067600.1; residues 443-799), human TrkB intracellular domain (NCBI NP_001018074.1; residues 455-822), and rat TrkC intracellular domain (NCBI NP_001257585.1; residues 454-864), respectively, into the OptoRaf1 KpnI and Kpn2I sites by Infusion-cloning. pFOS WT-GL3 was a gift from Ron Prywes (Addgene plasmid no. 11983). The Renilla luciferase control plasmid pRL-TK was obtained from Promega (cat. no. E2241).

Western blot

HEK293T cells were cultured in Dulbecco's modified Eagle's medium (DMEM) supplemented with 10% FBS and 1× Penicillin–Streptomycin solution (complete medium). Cultures were maintained in a standard humidified incubator at 37 °C with 5% CO_2. Transfection mixtures were prepared by combining 100, 200, 300, 400, 500, or 600 ng of the optoFGFR construct with of 1100, 1000, 900, 800, 700 ng, or 600 ng of the ICD-empty construct, respectively, in 120 µl DMEM containing 2.4 µg of polyethylenimine (PEI, PEI-to-DNA mass ratio of 2:1). The transfection mixtures were incubated at room temperature for 20 min prior to adding to cells cultured in 35-mm dishes with 1 ml complete medium. The transfection medium was replaced with 1 ml serum-free DMEM supplemented with 1× Penicillin–Streptomycin solution after 3 h of transfection to serum-starve cells overnight. Transfected and serum-starved HEK293T cells were treated with 10 mM Erlotinib (an EGFR inhibitor) for 5 min prior to illumination to further minimize baseline signaling. Cells were then illuminated for 5 min using a homemade blue LED light box emitting at 5 mW/cm^2. Control cultures remained in the dark during this time. Following illumination, cells were washed once with 1 ml cold DPBS and lysed with 100 µl cold lysis buffer (RIPA + protease/phosphatase inhibitor cocktail). Lysates were centrifuged at 17,000 RCF, 4 °C for 10 min to pellet cell debris. Purified lysates were normalized using Bradford reagent. Normalized samples were mixed with LDS buffer, heated at 95 °C for 5 min, and loaded onto 12% polyacrylamide gels. SDS-PAGE was performed at room temperature. Samples were transferred to PVDF membranes overnight at 30 V, 4 °C. Membranes were blocked in 5% BSA/TBST for 1 h at room temperature and probed with the primary and secondary antibodies according to company

guidelines. Membranes were incubated with ECL substrate and imaged using a Bio-Rad ChemiDoc XRS chemiluminescence detector.

Live-cell imaging for protein localization and PC12 cell differentiation

For light-mediated membrane translocation of cytosolic optoFGFR, HEK293T cells were transfected with CMT-OptoFGFR and recovered overnight before fluorescence imaging. For PC12 cell differentiation assay, transfected and recovered PC12 cells were switched to the starvation medium (F12K supplemented with 0.15% horse serum, 0.025% FBS, and 1× Penicillin–Streptomycin) immediately before incubating cells on a homemade blue LED light box with the light power at 400 μW/cm^2. Cells were incubated with light for 24 h before live-cell imaging with the EGFP fluorescence. An epi-illumination inverted fluorescence microscope (Leica DMI8) equipped with a 10× objective and a light-emitting diode illuminator (SOLA SE II 365) transfected cells. Green fluorescence was detected using the EGFP filter cube (Leica, excitation filter 472/30, dichroic mirror 495, and emission filter 520/35). The exposure time for both fluorescence channels was 200 ms. Confocal imaging was performed using a Zeiss LSM 700 microscope. Excitation beams were focused via a 60× dry objective. Ten pulses of 488-and 555-nm excitation light (5-s interval) were applied for CMT-OptoTrkC membrane translocation experiment.

Luciferase assays

Cells grown in the appropriate dishes were transiently transfected with the luciferase and control plasmids as explained in the figures and lysed after the indicated times by incubating with 1× passive lysis buffer and gently shaking at room temperature for 30 min. The lysate was centrifuged at maximum speed on a tabletop centrifuge (17,000 ***g***, 10 min), and the cleared supernatant was used for luciferase measurements in a Promega GloMax Luminometer (Promega cat. no. E5311) as per manufacturer recommendations.

Xenopus embryos and manipulations

Xenopus embryos were obtained and microinjections were performed as described [30]. When performing microinjection, embryos were placed in 0.5× Marc's Modified Ringer's with 3% Ficoll. RNA was injected into the ventral blastomeres of four-cell stage embryos using a Narishige IM300 microinjector. The dosage of RNA for microinjection is indicated in the text or figures. After injection, embryos were cultured in 0.2× Marc's Modified Ringer's and illuminated with blue light from the cleavage stage to the early neurula stage. Embryos were harvested at the tadpole stage and were imaged with a Leica M165 FC dissecting scope connected to a Leica DFC450 C digital camera using Leica Application Suite software v4.0. All *Xenopus* procedures were approved by the University of Illinois at Urbana–Champaign Institutional Animal Care and Use Committee under animal protocol #17199, and performed in accordance with the recommendations of the Guide for the Care and Use of Laboratory Animals of the National Institutes of Health.

Acknowledgements

Research reported in this publication was supported by the School of Molecular and Cellular Biology at UIUC, the National Institute of General Medical Sciences of the National Institutes of Health, and the National Institute of Environmental Health Sciences under Award Numbers R01GM132438 (K. Z.), R35GM131810 (J.Y.), and T32ES007326 (J.F.).

Appendix A. Supplementary data

Supplementary data to this article can be found online at https://doi.org/10.1016/j.jmb.2020.03.032.

Received 19 December 2019;
Received in revised form 26 March 2020;
Accepted 31 March 2020
Available online 8 April 2020

Keywords:
optogenetics;
RTK signaling;
differentiation;
ectopic tail;
Xenopus laevis

†V.V.K. and J.F. contributed equally to this work.

‡Current address: J. Khamo, Department of Biology, Elgin Community College, Elgin, IL 60123, USA.

Abbreviations used:
RTK, receptor tyrosine kinase; ICD, intracellular domain; PLCγ, phospholipase C γ; FGF, fibroblast growth factor; NGF, nerve growth factor; CRY2, cryptochrome 2; PHR, photolyase homology region; CIBN, cryptochrome-interacting basic helix–loop–helix N-terminal domain.

References

[1] M.A. Lemmon, J. Schlessinger, Cell signaling by receptor tyrosine kinases, Cell. 141 (2010) 1117–1134.

[2] D.M. Ornitz, N. Itoh, The fibroblast growth factor signaling pathway, Wiley Interdiscip. Rev. Dev. Biol. 4 (2015) 215–266.
[3] C.M. Teven, E.M. Farina, J. Rivas, R.R. Reid, Fibroblast growth factor (FGF) signaling in development and skeletal diseases, Genes Dis. 1 (2014) 199–213.
[4] I.N. Maruyama, Mechanisms of activation of receptor tyrosine kinases: monomers or dimers, Cells. 3 (2014) 304–330.
[5] A.M. Kopec, T.J. Carew, Growth factor signaling and memory formation: temporal and spatial integration of a molecular network, Learn. Mem. 20 (2013) 531–539.
[6] A. Levi, S. Alema, The mechanism of action of nerve growth factor, Annu. Rev. Pharmacol. Toxicol. 31 (1991) 205–228.
[7] R. Rydel, L. Greene, Acidic and basic fibroblast growth factors promote stable neurite outgrowth and neuronal differentiation in cultures of PC12 cells, J. Neurosci. 7 (1987) 3639–3653.
[8] J. Chung, H. Kubota, Y. Ozaki, S. Uda, S. Kuroda, Timing-dependent actions of NGF required for cell differentiation, PLoS One 5 (2010), e9011.
[9] S.P. Lad, D.A. Peterson, R.A. Bradshaw, K.E. Neet, Individual and combined effects of TrkA and p75NTR nerve growth factor receptors. A role for the high affinity receptor site, J. Biol. Chem. 278 (2003) 24808–24817.
[10] K. Susen, R. Heumann, A. Blochl, Nerve growth factor stimulates MAPK via the low affinity receptor p75(LNTR), FEBS Lett. 463 (1999) 231–234.
[11] K.Y. Chang, D. Woo, H. Jung, S. Lee, S. Kim, J. Won, et al., Light-inducible receptor tyrosine kinases that regulate neurotrophin signalling, Nat. Commun. 5 (2014) 4057.
[12] M. Grusch, K. Schelch, R. Riedler, E. Reichhart, C. Differ, W. Berger, et al., Spatio-temporally precise activation of engineered receptor tyrosine kinases by light, EMBO J. 33 (2014) 1713–1726.
[13] J.S. Khamo, V.V. Krishnamurthy, Q. Chen, J. Diao, K. Zhang, Optogenetic delineation of receptor tyrosine kinase subcircuits in PC12 cell differentiation, Cell Chem Biol. 26 (2019) 400–410(e3).
[14] N. Kim, J.M. Kim, M. Lee, C.Y. Kim, K.Y. Chang, W.D. Heo, Spatiotemporal control of fibroblast growth factor receptor signals by blue light, Chem. Biol. 21 (2014) 903–912.
[15] A.V. Leopold, K.G. Chernov, A.A. Shemetov, V.V. Verkhusha, Neurotrophin receptor tyrosine kinases regulated with near-infrared light, Nat. Commun. 10 (2019) 1129.
[16] S.K. Muthuswamy, M. Gilman, J.S. Brugge, Controlled dimerization of ErbB receptors provides evidence for differential signaling by homo- and heterodimers, Mol. Cell. Biol. 19 (1999) 6845–6857.
[17] B.E. Welm, K.W. Freeman, M. Chen, A. Contreras, D.M. Spencer, J.M. Rosen, Inducible dimerization of FGFR1: development of a mouse model to analyze progressive transformation of the mammary gland, J. Cell Biol. 157 (2002) 703–714.
[18] J. Yang, K. Symes, M. Mercola, S.L. Schreiber, Small-molecule control of insulin and PDGF receptor signaling and the role of membrane attachment, Curr. Biol. 8 (1998) 11–18.
[19] K. Csanaky, M.W. Hess, L. Klimaschewski, Membrane-associated, not cytoplasmic or nuclear, FGFR1 induces neuronal differentiation, Cells. 8 (2019).
[20] S.R. Agarwal, J. Gratwohl, M. Cozad, P.C. Yang, C.E. Clancy, R.D. Harvey, Compartmentalized cAMP signaling associated with lipid raft and non-raft membrane domains in adult ventricular Myocytes, Front. Pharmacol. 9 (2018) 332.
[21] D.A. Zacharias, J.D. Violin, A.C. Newton, R.Y. Tsien, Partitioning of lipid-modified monomeric GFPs into membrane microdomains of live cells, Science. 296 (2002) 913–916.
[22] M.J. Kennedy, R.M. Hughes, L.A. Peteya, J.W. Schwartz, M. D. Ehlers, C.L. Tucker, Rapid blue-light-mediated induction of protein interactions in living cells, Nat. Methods 7 (2010) 973–975.
[23] A. Ishimura, H.S. Lee, Y.S. Bong, C. Saucier, K. Mood, E. Park, et al., Oncogenic met receptor induces ectopic structures in Xenopus embryos, Oncogene. 25 (2006) 4286–4299.
[24] V.V. Krishnamurthy, J.S. Khamo, W. Mei, A.J. Turgeon, H.M. Ashraf, P. Mondal, et al., Reversible optogenetic control of kinase activity during differentiation and embryonic development, Development. 143 (2016) 4085–4094.
[25] L. Duan, J.M. Hope, S. Guo, Q. Ong, A. Francois, L. Kaplan, et al., Optical activation of TrkA signaling, ACS Synth. Biol. 7 (2018) 1685–1693.
[26] M.L. Donnelly, G. Luke, A. Mehrotra, X. Li, L.E. Hughes, D. Gani, et al., Analysis of the aphthovirus 2A/2B polyprotein 'cleavage' mechanism indicates not a proteolytic reaction, but a novel translational effect: a putative ribosomal 'skip', J Gen Virol. 82 (2001) 1013–1025.
[27] B. Cen, A. Selvaraj, R.C. Burgess, J.K. Hitzler, Z. Ma, S.W. Morris, et al., Megakaryoblastic leukemia 1, a potent transcriptional coactivator for serum response factor (SRF), is required for serum induction of SRF target genes, Mol. Cell. Biol. 23 (2003) 6597–6608.
[28] P. Monje, J. Hernandez-Losa, R.J. Lyons, M.D. Castellone, J.S. Gutkind, Regulation of the transcriptional activity of c-Fos by ERK. A novel role for the prolyl isomerase PIN1, J. Biol. Chem. 280 (2005) 35081–35084.
[29] A. Iimura, E. Nishida, M. Kusakabe, Role of TrkA signaling during tadpole tail regeneration and early embryonic development in *Xenopus laevis*, Genes Cells 25 (2) (2020) 86–99.
[30] H.L. Sive, R.M. Grainger, R.M. Harland, Early Development of *Xenopus laevis*: A Laboratory Manual, Cold Spring Harbor Laboratory Press, Cold Spring Harbor, NY, 2000.